Molecular Cancer Therapeutics

Modeling Dose and Schedule Effects of AZD2811 Nanoparticles Targeting Aurora B Kinase for Treatment of Diffuse Large B-cell Lymphoma

Nicolas Floc'h[1], Susan Ashton[2], Douglas Ferguson[3], Paula Taylor[2], Larissa S. Carnevalli[1], Adina M. Hughes[1], Emily Harris[2], Maureen Hattersley[5], Shenghua Wen[5], Nicola J. Curtis[2], James E. Pilling[4], Lucy A. Young[1], Kim Maratea[6], Elizabeth J. Pease[7], and Simon T. Barry[1]

Abstract

Barasertib (AZD1152), a pro-drug of the highly potent and selective Aurora B kinase inhibitor AZD2811, showed promising clinical activity in relapsed/refractory diffuse large B-cell lymphoma (DLBCL) patients administered as a 4-day infusion. To improve potential therapeutic benefit of Aurora B kinase inhibition, a nanoparticle formulation of AZD2811 has been developed to address limitations of repeated intravenous infusion. One of the challenges with the use of nanoparticles for chronic treatment of tumors is optimizing dose and schedule required to enable repeat administration to sustain tumor growth inhibition. AZD2811 gives potent cell growth inhibition across a range of DLBCL cells lines i*n vitro*. *In vivo*, repeat administration of the AZD2811 nanoparticle gave antitumor activity at half the dose intensity of AZD1152. Compared with AZD1152, a single dose of AZD2811 nanoparticle gave less reduction in pHH3, but increased apoptosis and reduction of cells in G1 and G_2–M, albeit at later time points, suggesting that duration and depth of target inhibition influence the nature of the tumor cell response to drug. Further exploration of the influence of dose and schedule on efficacy revealed that AZD2811 nanoparticle can be used flexibly with repeat administration of 25 mg/kg administered up to 7 days apart being sufficient to maintain equivalent tumor control. Timing of repeat administration could be varied with 50 mg/kg every 2 weeks controlling tumor control as effectively as 25 mg/kg every week. AZD2811 nanoparticle can be administered with very different doses and schedules to inhibit DLBCL tumor growth, although maximal tumor growth inhibition was achieved with the highest dose intensities.

Introduction

Diffuse large B-cell lymphoma (DLBCL) is the most prevalent form of adult lymphoma (1). There are two major biologically distinct molecular subtypes: germinal center B-cell (GCB) and activated B-cell (ABC) (2, 3). There has been little progress developing new therapies. Standard of care for DLBCL remains chemotherapy based, usually with a regimen of 4 drugs (cyclophosphamide, doxorubicin, vincristine, and prednisone) combined with immunotherapy using a chimeric mAb against the protein CD20 (rituximab), R-CHOP (4). Unfortunately, approximately 40% of patients treated under this regimen will have disease that is either refractory or will relapse following initial response (5). The average patient age is 65 years old and usually therefore intensive chemotherapy is challenging (6); hence, the development of new treatment options is critical.

Analysis of the genetic basis underlying DLBCL's pathogenesis has led to the identification of critical biological programs and central signaling pathways that could be exploited for therapeutic intervention (7). Agents targeting the NF-κB pathway (IκBα inhibitor; ref. 8) or the B-cell receptor signaling pathway (BTK or SYK inhibitors) (9, 10) are under evaluation and hold the most promise for treating ABC DLBCL. Agents targeting the PI3K/AKT/MTOR pathway (11), Bcl-2 inhibitors (12), or EZH2 inhibitors (13, 14) are also under evaluation for treatment of GCB DLBCL.

Given the aggressive hyperproliferative nature of DLBCL, it is thought progressive disease would be sensitive to agents targeting the cell-cycle machinery. A number of cell-cycle inhibitors have been developed as antimitotic agents. Barasertib (AZD1152) is a pro-drug that rapidly undergoes phosphatase-mediated cleavage in plasma following intravenous administration to release AZD2811 (formerly known as AZD1152-hQPA), a highly potent and selective Aurora B kinase inhibitor (15–19). It is proposed that inhibition of Aurora B kinase induces chromosome misalignments during mitosis and failed cytokinesis leading to polyploidization and to cell death (20). However, there is heterogeneity in cell responses to Aurora B kinase inhibition as some cells can undergo rapid apoptosis with minimal polyploidy, and other persist with polyploid nuclei. Barasertib has shown promising

[1]Bioscience, Oncology, IMED Biotech Unit, AstraZeneca, Cambridge, United Kingdom. [2]Bioscience, Oncology, IMED Biotech Unit, AstraZeneca, Macclesfield, United Kingdom. [3]Oncology DMPK, IMED Biotech Unit, AstraZeneca, Boston, United States. [4]Bioscience, Oncology, IMED Biotech Unit, AstraZeneca, Boston, United States. [5]Discovery Sciences, Oncology, IMED Biotech Unit, AstraZeneca, Cambridge, United Kingdom. [6]IMED Drug Safety & Metabolism, AstraZeneca, Gatehouse Park, Waltham, Boston, United States. [7]Projects, Oncology IMED, AstraZeneca, Cambridge, United Kingdom.

Note: Supplementary data for this article are available at Molecular Cancer Therapeutics Online (http://mct.aacrjournals.org/).

Corresponding Author: Nicolas Floc'h, AstraZeneca, Robinson Way, Cambridge CB2 0RE, United Kingdom. Phone: 122-376-9654; Simon T. Barry, Phone: 778-974-4771; E-mail: simon.t.barry@astrazeneca.com

doi: 10.1158/1535-7163.MCT-18-0577

benefits in phase II clinical trials in relapsed/refractory DLBCL patients, with an improvement of the overall response rate by approximately 20% (21). However, the inconvenience of the mode of administration as a 4-day infusion has prevented further exploration and development of barasertib. To address this challenge, a nanoparticle encapsulating AZD2811 has been developed (15).

This study examines the preclinical activity of AZD2811 nanoparticle formulation in DLBCL cell lines and tumor models, and moreover how the nanoparticle can be delivered using different doses and schedules to achieve consistent antitumor activity.

Materials and Methods

In vitro studies

DB (origin: ATCC, CRL-2289) and Su-DHL-8 (origin: DSMZ, ACC-573) cell lines were cultured and assayed in RPMI1640 phenol red-free media supplemented with 20% v/v FCS and 2 mmol/L L-glutamine. HT (origin: ATCC, CRL-2260), Karpass-422 (origin: DSMZ, ACC-32), RC-K8 (origin: DSMZ, ACC-561), Su-DHL-4 (origin: DMZ, ACC-495), and Su-DHL-6 (origin: DSMZ, ACC-572) cell lines were cultured and assayed in RPMI1640 phenol red-free media supplemented with 15% v/v FCS and 2 mmol/L L-glutamine. The remainder of the cell lines, OCI-LY19 (origin: DMZ, ACC-528), DOHH2 (origin: DSMZ, ACC-47), RI-1 (origin: DSMZ, ACC-585), Raji (origin: ATCC, CCL-86), TMD-8 (origin: Prof. Daniel Krappmann's lab), Pfeiffer (origin: ATCC, CRL-2632), Su-DHL-10 (origin: DSMZ, ACC-576), WSU-DLCL-2 (origin: DSMZ, ACC-575), and U2932 (origin: DMZ, ACC-633) were cultured and assayed in RPMI1640 phenol red-free supplemented with 10% v/v FCS + 2 mmol/L L-glutamine. All cell lines were maintained and assayed under humidified conditions of 37°C and 5% CO_2. All cell lines were authenticated at AstraZeneca cell banking using DNA fingerprinting short tandem repeat (STR) assays and confirmed to be free of bacterial and viral contaminations by IDEXX. All cell lines were used within 15 passages, and less than 6 months.

Cells were seeded in 96-well plates at a density allowing for logarithmic growth during the 6 days assay. Cells were exposed to an AZD2811 (AZD1152-hQPA) monotherapy dose response. Following 6-day compound incubation, cell viability was assessed through the addition of Alamar Blue reagent. The reaction was stopped with 0.5% SDS solution and fluorescence read on a Tecan Saffire II. The dose at which 50% inhibition of viability (IC_{50}) was achieved was established for each cell line. For assessment of nuclear area, cells were stained with Hoescht (1:1000) in RPMI1640, pipetting the cells up and down 3 times to disperse any clumps. After 20 minutes, the plates were centrifuged at 300 × *g* for 5 minutes. Five images per well at ×20 magnification were taken for assessment of nuclear area.

In vivo studies

All animal studies were conducted in accordance with U.K. Home Office legislation, the Animal Scientific Procedures Act 1986, as well as the AstraZeneca Global Bioethics policy. All experimental work is outlined in project licence 40/3483, which has gone through the AstraZeneca Ethical Review Process. Studies in the United States were conducted in accordance with the guidelines established by the internal IACUC (Institutional Animal Care and Use Committee) and reported following the ARRIVE (Animal Research: Reporting *In Vivo* Experiments) guidelines (22). Randomization of animals onto study was based on initial tumor volumes to ensure equal distribution across groups. A power analysis was performed whereby group sizes were calculated to enable statistically robust detection of tumor growth inhibition (>6/group) or pharmacodynamic endpoint (>4/group).

Tumor growth inhibition studies in tumor xenograft models

All animals included on studies were greater than 5 to 6 weeks old at the time of cell implant. Human DLBCL OCI-LY19 were cultured in RPMI supplemented with 20% v/v FCS and 1% v/v L-glutamine (Invitrogen) and cultured in a humidified incubator with 5% CO_2 at 37°C. OCI-LY19 xenografts were established by subcutaneous implantation of 1×10^7, cells per animal, in 100 μL of cell suspension including 50% Matrigel, into the dorsal left flank of female CB17 SCID mice. Human DLBCL U2932 Luc2 were cultured in RPMI supplemented with 10% v/v FCS, 1% v/v L-glutamine and 500 μg/mL geneticin and cultured in a humidified incubator with 5% CO_2 at 37°C. U2932 Luc2 xenografts were established by tail vein injection of 1×10^7 per animal in 200 μL of cell suspension, of female SCID Beige mice. Randomization for animal studies was based on initial tumor burden to ensure equal distribution across groups. Tumors were measured two to three times weekly by caliper and volume calculated using elliptical formula (pi/6 × width × width × length). Tumor growth inhibition (%TGI) from the start of treatment was assessed by comparison of the geometric mean change in tumor volume for the control and treated groups. Tumor regression was calculated as the percentage reduction in tumor volume from baseline value: % Regression = (1 − RTV) × 100 % where RTV = Geometric Mean Relative Tumor Volume. Statistical significance was evaluated using a one-tailed *t* test.

Xenogen IVIS imaging

The U2932 Luc2 model was monitored by bioluminescent imaging assessment of luciferase activity as a marker of tumor burden. Tumor response to therapy was followed using the Xenogen IVIS 200 Imaging technology. To enable visualization of tumors, intraperitoneal injection of D-luciferin potassium salt (15 mg/mL dosed at 10 mL/kg) was given approximately 10 to 15 minutes prior to imaging. Following intraperitoneal injection, the animals were anesthetized using Isoflurane anesthesia. Anesthesia was maintained with 1.0% to 3.0% isoflurane in 100% oxygen throughout the imaging process. Images were then acquired using the Living Image 2.6 software program, and the imaging data represented as total photons.

Pharmacodynamic studies in tumor xenograft models

For pharmacodynamic studies, mice were randomized at a tumor volume around 0.5 cm^3 using the same randomization criteria as the tumor growth inhibition studies. SCID mice bearing OCI-LY19 xenografts were then dosed intravenously with a single bolus dose of placebo nanoparticles, AZD2811 nanoparticle or AZD1152. Tumors were excised postmortem at specified time points and flash frozen in liquid nitrogen for FACS analysis or fixed in 10% buffered formalin for 24 to 48 hours, and then processed to paraffin block for IHC. Frozen tumors were disaggregated in cold PBS using Medicon Technology and fixed in 80% ethanol. Resulting cell suspensions were blocked with 1% BSA

before incubation with primary antibody to pHH3 (Millipore) and subsequent incubation with a fluorescein isothiocyanate (FITC)–conjugated anti-rabbit IgG (H+L) secondary antibody (Millipore). Finally, cells were incubated with ribonuclease (1 mg/mL) (Sigma) and propidium iodide (0.4 mg/mL; Sigma) and analyzed by flow cytometry. Activity was measured as an inhibition of histone H3 phosphorylation on Ser10. Average numbers of pHH3 positive cells in G_2–M were calculated for each treatment group and compared to the pHH3 level in G_2–M phase cells from the placebo nanoparticle group. Flow cytometry analysis was performed on a BD ARIA I flow cytometer. FACS data was analyzed with FlowJo software (Treestar) and processed using GraphPad Prism 6 (GrapPad Software). For IHC, sections (4 μm) were deparaffinized with xylene and rehydrated through graded alcohols into water. Antigen retrieval was carried out in a Milestone RHS microwave rapid histoprocessor for 5 minutes at 110°C in pH 6 citrate buffer (Dako S1699). Tissues were placed on a Lab Vision Autostainer, endogenous peroxidase was blocked with 3% H_2O_2 for 10 minutes, followed by washing twice in TBS/0.05% Tween (TBS-T). For phosphohistone H3 (pHH3), serum-free protein block (Dako; X0909) was applied for 15 minutes prior to incubation with primary antibody (Upstate Biotechnology 06-570; 1/1,000 dilution) for 1 hour. For detection of pHH3, sections were incubated for 30 minutes with Rabbit EnVision polymer detection system (Dako; K4003). Samples were developed in liquid 3,3-diaminobenzidine (DAB;Dako K3468) for 10 minutes. Sections were then counterstained with Carazzi hematoxylin, dehydrated, cleared, and mounted with coverslips. All washes were performed in TBS-T and all steps were conducted at room temperature. pHH3 immunoreactivity were scored semi-quantitatively by a pathologist as follows: 0 = <5% positive cells; 1 = 5%–10% positive cells; 2 = 11%–25% positive cells; 3 = 26%–50%; 4 $^1/_4$ >50% positive cells. Hematoxylin and eosin (H&E)-stained sections were scored for karyomegaly, an indicator of polyploidy, using the same system.

Pharmacokinetic studies in tumor xenograft models

Pharmacokinetic studies were performed in female nude mice. AZD2811 nanoparticle (AZD2811NP) or nonencapsulated AZD2811 were dosed by intravenous bolus (at 25 and 5 mg/kg, respectively) and terminal blood samples obtained at a series of time points ranging from 5 minutes to 196 hours.

Blood samples were centrifuged at 13,000 rpm for 3 minutes at 3°C to 4°C. Plasma was removed and stored at −80°C before analysis. Subsequent steps were carried out on ice. Plasma samples (25 μL) were diluted using an appropriate dilution factor. Acetonitrile (100 μL) was added with the internal standard, followed by centrifugation at 3,000 rpm for 10 minutes. Supernatant (50 μL) was then diluted in 300 μL water and analyzed via UPLC-MS/MS against an 11-point standard calibration curve (1–10,000 nmol/L). LC/MS-MS conditions are listed in Supplementary Tables S1 and S2.

Pharmacokinetic model

All model fitting was performed using WinNonlin Phoenix 6.4 using naïve pooled approach. Systemic pharmacokinetics of nonencapsulated (or released) AZD2811 were modeled using a 2-compartment model. Estimated parameter values are listed in Supplementary Table S3. For AZD2811NP dosed mice, the release of AZD2811 from the nanoparticles was assumed to be a diffusion-based process and was modeled using the equation below (as described in ref. 23):

$$\frac{d(AZD2811NP)_{body}}{dt} = \frac{-K_{diff} \times (AZD2811NP)_{body}}{t^{\gamma}}$$

where $(AZD2811NP)_{body}$ refers to the amount of nanoparticle encapsulated AZD2811 in the body at time t, K_{diff} is the effective constant of diffusion and γ is the diffusion versus time factor (estimated values 0.024 hr^{-1} and 0.24, respectively). It was assumed that all drug in the AZD2811NP formulation was encapsulated at $t = 0$ and that the full AZD2811 payload would eventually be released into blood and tissues.

Concentrations of nonencapsulated AZD2811 in plasma following multiple dosing were simulated using the pharmacokinetic model developed from single dose pharmacokinetic studies. Free (nonprotein bound) fraction in plasma was determined by equilibrium dialysis (free fraction = 0.09) and used to convert the simulated total plasma concentration of nonencapsulated AZD2811 into free concentration.

All *in vivo* studies were dosed intravenously with placebo nanoparticles, AZD1152 or AZD2811 nanoparticle. The nanoparticles were diluted to required concentration in 0.9% physiologic saline. AZD1152 was diluted to required concentration in 0.3 mol/L Tris buffer, pH9.

Results

In vitro AZD2811 reduces proliferation and induces polyploidy across a panel of human DLBCL cancer cell lines

To evaluate the cytotoxic and antiproliferative effects of AZD2811, an alamarBlue assay was performed in a panel of 17 DLBCL cell lines treated with 0 to 3,000 nmol/L of AZD2811 for 6 days. The concentration of AZD2811 resulting in 50% growth inhibition (IC_{50}) when compared with the control was determined and converted into pIC_{50}. Nine out of 17 DLBCL cell lines were highly sensitive to AZD2811 with a pIC_{50} greater than 8 (IC_{50} <10 nmol/L; Fig. 1A; Supplementary Table S4). Six DLBCL cell lines were moderately sensitive to AZD2811 with a pIC_{50} between 8 and 7.5 (10 nmol/L < IC_{50} < 30 nmol/L; Fig. 1A; Supplementary Table S4). Two cell lines showed low sensitivity to AZD2811 with pIC_{50}s lower than 7.5 (IC_{50} = 100 nmol/L; Fig. 1A; Supplementary Table S4). Consistent with the expected mechanism of action, AZD2811 increased nuclear area, up to 2.9-fold at day 6 (Fig. 1B). Increased nuclear size is commonly associated with polyploidy a consequence of Aurora B kinase inhibition. Interestingly across the panel, the phenotypic consequences were variable relative to the effect on cell proliferation or survival. The correlation between pIC_{50} and nuclear area was not consistent, especially for the cells most sensitive to AZD2811. In some of the most sensitive cell lines, this may be because AZD2811 rapidly induced apoptosis once the cell develops polyploidy. Overall, these data suggested that AZD2811 has the potential for broad antitumor activity in DLBCL cancer cell lines.

Half the dose intensity of AZD2811 nanoparticle relative to AZD1152 reduces growth of the subcutaneous OCI-LY19 and disseminated U2932Luc2 DLBCL tumor xenografts

We previously showed that a single cycle of AZD2811 administered on day 1 and 3 delivered antitumor activity (15). To

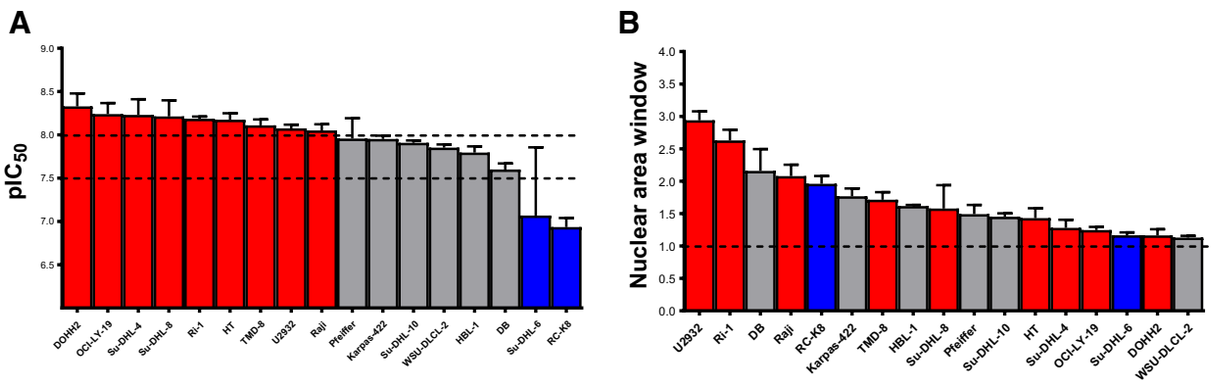

Figure 1.

AZD2811 reduces proliferation and induces polyploidy across a panel of human DLBCL cell lines *in vitro*. **A,** Bar graph representing cell proliferation data displayed as pIC_{50} values. **B,** Bar graph representing increased in polyploidy cells displayed as nuclear area window. Data are represented as mean ± SEM ($n = 3$–6).

address effects of long-term administration multiple cycles of treatment were assessed. Two cycles of AZD2811 nanoparticle resulted in comparable tumor growth inhibition to AZD1152 when AZD2811 was administered at half the dose intensity (total amount of drug given in a fixed unit of time) of AZD1152 (95% and 93% TGI respectively relative to the placebo nanoparticle group at day 15 ($P > 0.001$) in the subcutaneous OCI-LY19 xenograft model (Fig. 2A). At these doses and schedules, both AZD1152 and AZD2811 nanoparticle were well tolerated with minimal body weight loss (less than 10% of starting body weight; Fig. 2B). Efficacy of the AZD2811 nanoparticle was also explored in the disseminated xenograft model U2932 Luc2. U2932 cells were sensitive to AZD2811 *in vitro* with treatment increasing nuclear area, and reduction in cell proliferation. In this model, DLBCL cells expressing the luciferase reporter gene Luc2 are introduced intravenously and proliferate in the blood. Similarly, two cycles of AZD2811 nanoparticle given at half of the dose intensity of AZD1152 was sufficient to induce a similar delay of the growth of the tumor cells in the blood when compared with the control group (Fig. 2C; Supplementary Fig. S1). In these mice, AZD2811 nanoparticle was well tolerated at 25 mg/kg; no body weight loss was observed initially compared with predose start body weight, whereas the control group lost weight as a result of the rapid increase in tumor burden (Fig. 2D). These data establish that the nanoparticle is effective in both solid tumor lesion and disseminated tumor cells.

AZD2811 nanoparticle induces apoptosis in subcutaneous OCI-LY19 xenografts

Using the OCI-LY19 model, the impact of AZD2811 nanoparticle on the mechanistic biomarkers of pHH3 inhibition, cell-cycle distribution, and apoptosis was examined. Following administration of AZD1152, we observed a rapid reduction of pHH3 level and an increase of polyploidy at 6 hours, with recovery to baseline at the 48 h timepoints (Fig. 3A and B). In contrast, in tumors treated with AZD2811 nanoparticles, the effect on pHH3 level was delayed and the induction of polyploidy in the whole cell population was less pronounced despite induction of apoptosis (Fig. 3A–C; Supplementary Fig. S2). Moreover, the effects of AZD2811 nanoparticle were dose dependent (Fig. 3A–C). This is consistent with the slow release pharmacokinetic profile of the nanoparticle (20). The difference in activity in between AZD1152 and AZD2811 nanoparticle can be explained by increased apoptosis with the high dose of AZD2811 nanoparticle. Indeed, high doses of AZD2811 nanoparticle increased the percentage of the apoptotic sub-G_0 population in the tumors (Fig. 3C–E). Collectively, the data suggest that sustained exposure with AZD2811 following nanoparticle administration drives persistent disruption of the cell cycle and increased apoptosis.

Total dose of AZD2811 nanoparticle delivered with different schedules determines antitumor activity in the subcutaneous OCI-LY19 DLBCL xenograft model

To understand the flexibility with which the AZD2811 nanoparticle can be administered to deliver optimal efficacy, different schedules were explored. Although this is critical to guide optimal clinical development, support long-term dosing, and ability to combine with other therapies, it is not commonly examined for nanoparticle formulations. Three different schedules were compared: administration of AZD2811 nanoparticle on day 1 and day 3 every 2 weeks, administration on day 1 and day 5 every 2 weeks, and weekly administration on day 1 of each week. AZD2811 nanoparticle induced very similar TGI with each of these schedules (95%, 95%, and 94%, respectively, at day 15, $P > 0.001$) relative to the placebo nanoparticle group (Fig. 4A). The similar TGI may be explained by the pharmacokinetic model (Fig. 4B), which indicates that the rate of release of AZD2811 from the nanoparticle is sufficient to maintain free concentration of AZD2811 in plasma above the OCI-LY19 *in vitro* IC_{50}; (pIC_{50} of 8.24 equivalent to IC_{50} of 5.7 nmol/L; Fig. 1A; Supplementary Tables S4 and S5) almost throughout the two week dosing interval for all three dose schedules (Fig. 4B).

When given as a single dose of 50 mg/kg every 2 weeks or at 25 mg/kg weekly, AZD2811 nanoparticle also induces a very similar effect (9% tumor regression and 99% TGI, respectively, at day 15, $P > 0.001$) relative to the placebo nanoparticle group (Fig. 4C). Again, *in vivo* antitumor efficacy appears to be consistent with the modelled time course of free AZD2811 concentration in

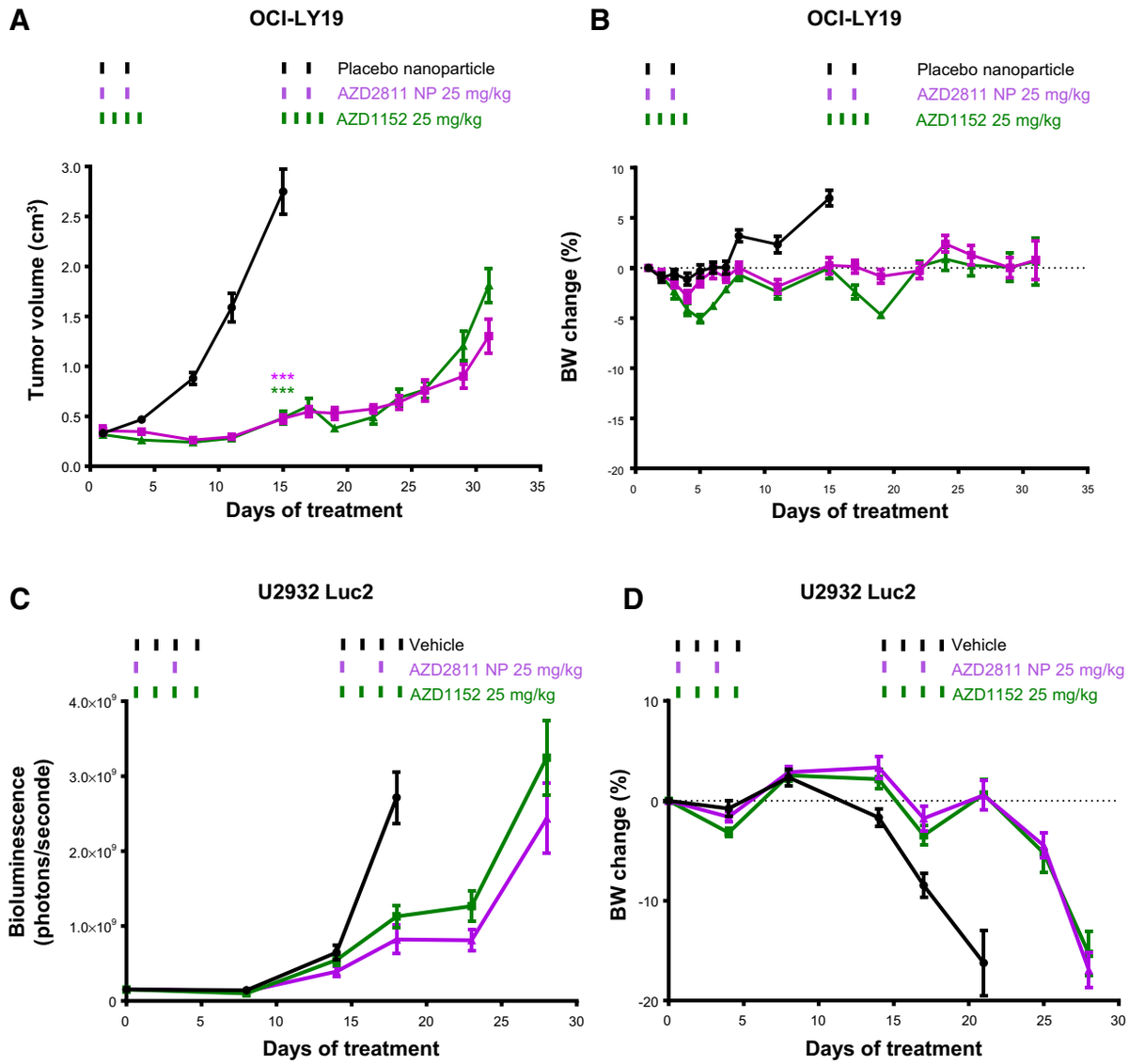

Figure 2.

AZD2811 nanoparticle is more potent than AZD1152 in the subcutaneous OCI-LY19 and the disseminated U2932Luc2 DLBCL xenograft model *in vivo*. **A,** Tumor growth inhibition after two cycles of the AZD2811 nanoparticle delivered at half the dose intensity of AZD1152 in the subcutaneous OCI-LY19 xenograft model in CB17 SCID mice. **B,** Percentage changes in body weight relative to start size on day 0 of SCID mice bearing OCI-LY19 subcutaneous xenograft model following two cycles of AZD1152 or AZD2811 nanoparticle ($n = 12$ for placebo nanoparticle and $n = 7$ or 8 for AZD2811 nanoparticle-treated groups). **C,** Tumor growth inhibition after two cycles of the AZD2811 nanoparticle or AZD1152 monotherapy treatment in the disseminated U2932 Luc2 xenograft model in SCID beige mice. Tumor burden is monitored by bioluminescent imaging. **D,** Percentage changes in body weight relative to start size on day 0 of SCID beige mice tail vein injected with the U2932 Luc2 disseminated xenograft model. Data are represented as mean ± SEM ($n = 10$/group treatment). Statistical significance was evaluated using a one-tailed *t*-test (***, $P > 0.001$).

plasma. During the first week, higher concentrations are achieved following the 50 mg/kg dose, resulting in a slightly greater reduction in tumor volume (relative to the 25 mg/kg group). This is offset during the second week where, for the 50 mg/kg group, plasma concentration continues to decline ($\leq IC_{50}$) and modest regrowth begins to be observed (~day 11–day 15). In contrast, the second 25 mg/kg dose on day 8 maintains free concentrations above the IC_{50}, preventing regrowth during the second week and resulting in an overall similar level of activity at the start of the next cycle of dosing (day 15; Fig. 4D).

At the different doses and schedules explored, AZD2811 nanoparticle was well tolerated, and minimal body weight loss (less than 10% of starting body weight) was observed (Supplementary Fig. S3A and S3B). The data in Fig. 4 suggest that a similar total dose of AZD2811 nanoparticle delivered over a time period using different schedules provides a very similar TGI.

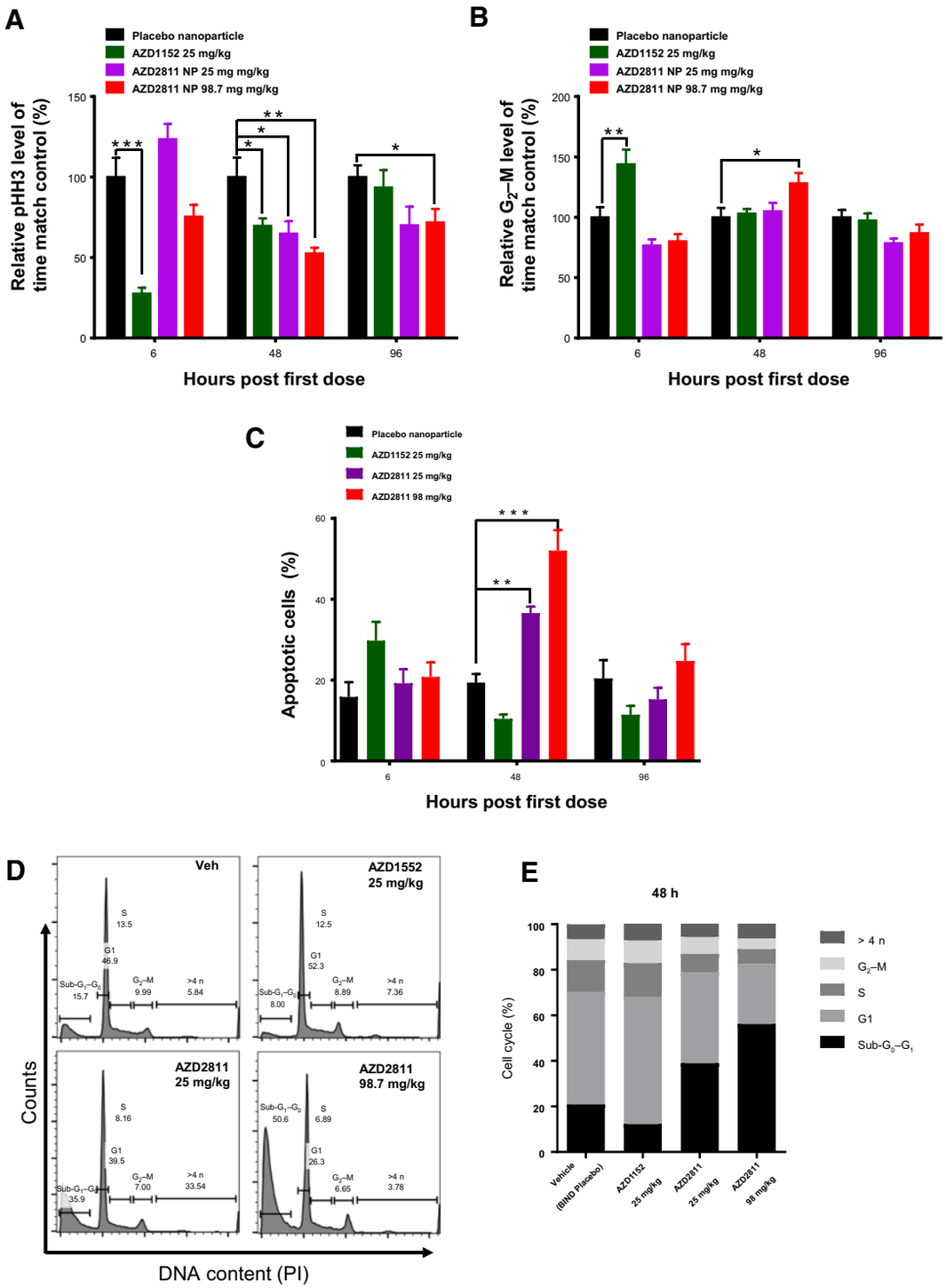

Figure 3.

AZD2811 nanoparticle induces apoptosis in the subcutaneous DLBCL OCI-LY19 xenograft models. **A,** Bar graph representing the relative pHH3 level of time match control (%) from tumors collected at 6, 48, and 96 hours following the first dose of AZD2811 nanoparticle or AZD1152. **B,** Bar graph representing the relative G_2–M level of time match control (%) from tumors collected at 6, 48, and 96 hours following the first dose of AZD2811 nanoparticle or AZD1152. In the figure, data are represented as mean tumor volumes ± SEM ($n = 5$ for control and treated group). **C,** Bar graph representing timecourse relative percentage of apoptotic cells in sub-G_0 cell-cycle phase in tumors collected at 6, 48, and 96 hours following the first dose of AZD2811 nanoparticle or AZD1152. **D** and **E,** Representative flow cytometry histograms (**D**) and normalized percentages of cell-cycle distribution across treatments 48 hours after initial dose of inhibitors (**E**). Data are represented as mean ± SEM ($n = 5$/group). Statistical analysis is a by one-way ANOVA.

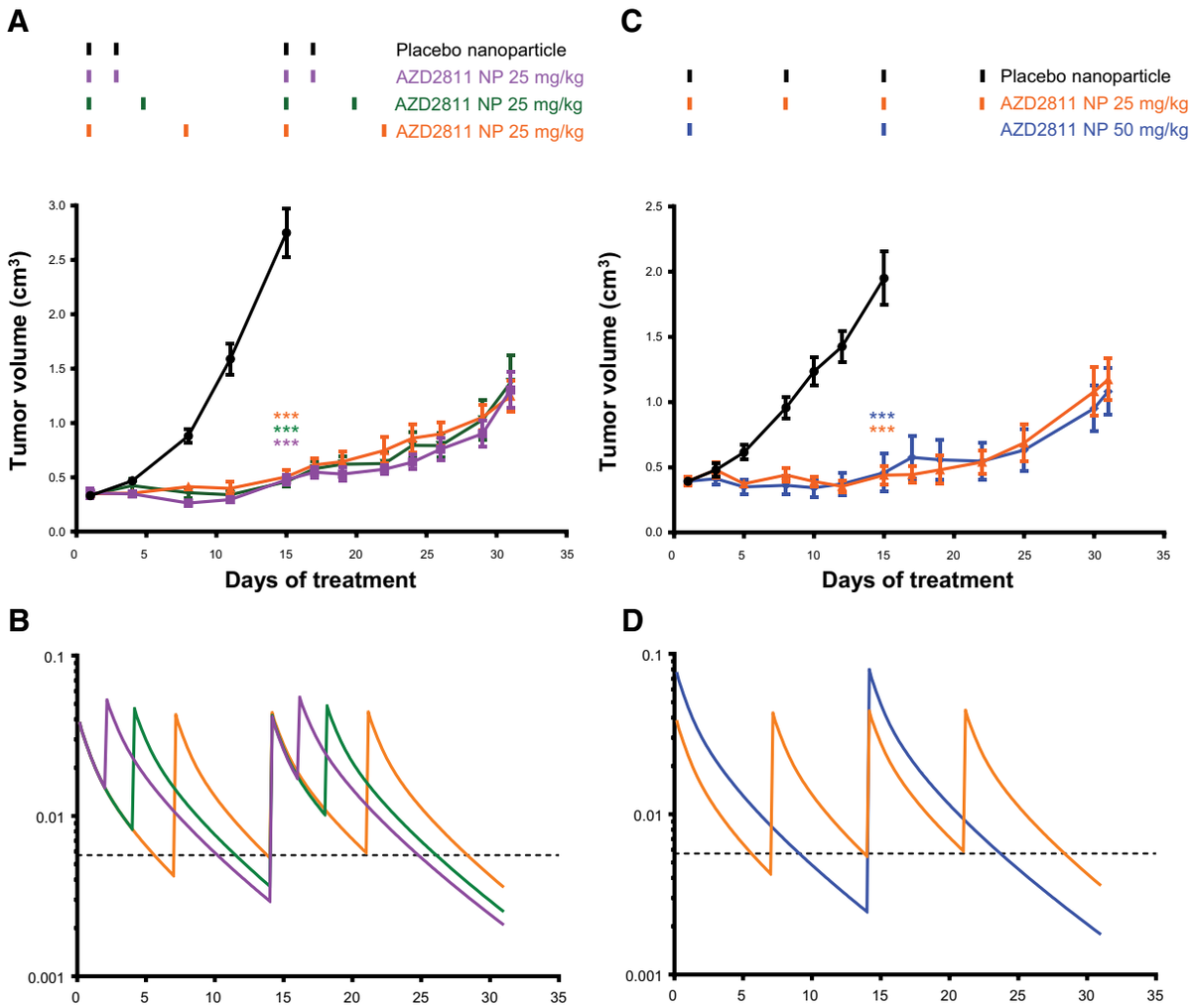

Figure 4.

AZD2811 nanoparticle delivered at a similar total dose through various schedule induces similar effect on the growth of the subcutaneous OCI-LY19 DLBCL xenograft model *in vivo*. **A** and **B,** Tumor growth inhibition (**A**) and predicted released free concentration profile (**B**) after two cycles of AZD2811 nanoparticle dosed at 25 mg/kg on D1/D3 or D1/D5 or D1/D8. **C** and **D,** Tumor growth inhibition (**C**) and predicted released free concentration profile (**D**) after dosing of AZD2811 nanoparticle at 25 mg/kg weekly or at 50 mg/kg every two weeks in the subcutaneous OCI-LY19 xenograft model in CB17 SCID mice. Tumor growth inhibition data are represented as mean ± SEM ($n = 12$ for placebo nanoparticle and $n = 7$ or 8 for AZD2811 nanoparticle-treated groups). Statistical significance was evaluated using a one-tailed *t*-test (***, $P > 0.001$).

Increasing the dose of AZD2811 nanoparticle increases the durability of response in the subcutaneous OCI-LY19 DLBCL xenograft model

To establish whether increasing the dose will give greater durability of response, mice bearing OCI-LY19 DLBCL xenografts were treated weekly with different doses of AZD2811 nanoparticle. A weekly dose of 25 mg/kg of AZD2811 nanoparticle resulted in 99% TGI relative to the placebo nanoparticle group control tumors at day 15 ($P > 0.001$). Moreover, a weekly dose of 50 or 98.7 mg/kg of AZD2811 nanoparticle resulted in 42% and 66% tumor regression respectively relative to the tumor size at the start of treatment (Fig. 5A). Pharmacokinetics were modeled to be linear over this dose range, and the dose-proportional increases in free concentration of AZD2811 at 50 and 98.7 mg/kg would be consistent with greater target inhibition throughout the course of the study (Fig. 5B; Supplementary Table S5). At the different doses and schedules explored, AZD2811 nanoparticle formulation was well tolerated, and minimal body weight loss (less than 10% of starting body weight) was observed (Supplementary Fig. S3C).

The impact of reduced dosing frequency on tumor control was also explored. Reduction in the frequency of dosing correlated with a reduction in efficacy (Fig. 6). A dose of 50 mg/kg of AZD2811 nanoparticle delivered weekly (2 doses), every 2 weeks (1 dose) or every 3 weeks (1 dose) gave 42%, 9%, and 6% regression at day 15 ($P > 0.001$; Fig. 6A). AZD2811 nanoparticle delivered every 2 weeks or every 3 weeks look very similar up to day 15 as only one dose was delivered, but the delivery of a second dose at day 15 in the 2-week schedule maintained tumor control. In contrast, the tumor regrowth was observed in the every three

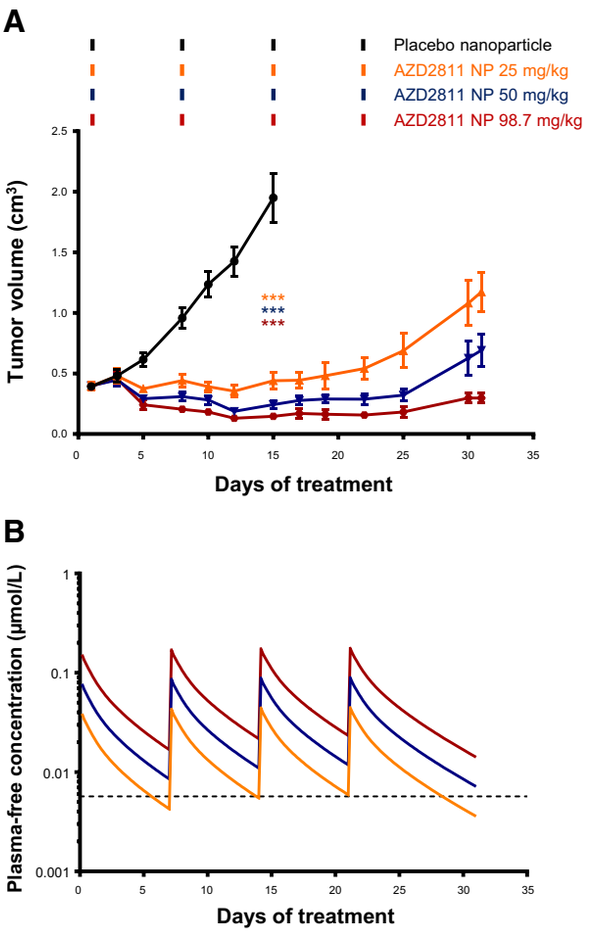

Figure 5.

AZD2811 nanoparticle induces dose-dependent tumor growth inhibition in the OCI-LY19 DLBCL xenograft model *in vivo*. **A,** Dose-related tumor growth inhibition after 4 cycles of the AZD2811 nanoparticle in the subcutaneous OCI-LY19 xenograft model in CB17 SCID mice. **B,** Predicted released free concentration profile of 4 cycles of the AZD2811 nanoparticle administrated at various doses in the subcutaneous OCI-LY19 xenograft model in CB17 SCID mice. Tumor growth inhibition data are represented as mean ± SEM ($n = 12$ for placebo nanoparticle and $n = 7$ or 8 for AZD2811 nanoparticle-treated groups). Statistical significance was evaluated using a one-tailed *t*-test (***, $P > 0.001$).

weekly schedule (Fig. 6A). A dose of 98.7 mg/kg (maximum deliverable dose) of AZD2811 nanoparticle delivered weekly (3 doses), every 2 weeks (2 doses) or every 3 weeks (1 dose) gave 63%, 37%, and 2% regression respectively at day 22 ($P >$ 0.001; Fig. 6B). The reduction in efficacy observed with reduced dosing frequency can be explained by the pharmacokinetic model, which suggests that the release rate from the nanoparticle is only sufficient to maintain the free concentration of AZD2811 in plasma above the IC_{50} for approximately 11 days following a 50 mg/kg dose (Fig. 6C; Supplementary Table S5) and approximately 15 days following a 98.7 mg/kg dose (Fig. 6D; Supplementary Table S5). Net tumor regrowth commences at these times (as normal cytokinetic events begin to outweigh failed cytokinesis) unless a second dose has been administered. Delaying subsequent doses allows periods of net tumor growth which leads to a reduction in the overall extent of regression observed at the end of the study. Collectively, these data show that the dose intensity of treatment will impact the durability of the response and that both dose and schedule considerations are critical to maintain durable responses.

Discussion

The preclinical data presented here support the potential for the Aurora B kinase inhibitor AZD2811 nanoparticle formulation as a new therapeutic for DLBCL. Moreover, we have established that the dose and schedule with which the nanoparticle is administered is important for tumor response and durable efficacy.

In vitro, AZD2811 reduced DLBCL cell proliferation, with the majority of the DLBCL cell lines being inhibited at low concentrations (IC_{50} < 30 nmol/L). Consistent with previous studies (15), despite the limited number of ABC cell lines represented in panel AZD2811 did not show marked differences in efficacy between ABC and GCB subtypes. AZD2811 induces an increase in the nuclear area consistent with the increase in polyploidy expected to be induced by an Aurora B kinase inhibitor. Interestingly, although it is commonly thought that the inhibition of Aurora B kinase results in stepwise increase in nuclear area and accumulation of polyploidy, the response across the cell panel varied between cell lines. Indeed, in some cell lines, AZD2811 reduced proliferation with little impact on nuclear area. It is possible that some cells, more sensitive to disruption of the Aurora B kinase function, enter apoptosis faster and hence are not represented in the analysis, while less sensitive cells exhibit greater accumulation of the nuclear phenotype change, which might not always lead to rapid apoptosis. In addition, cell death may not necessarily occur through inhibition of a canonical Aurora B kinase signaling. Recently, a noncanonical dependency for Aurora B kinase function was described for SCLC cell lines in which the RB tumor suppressor function is lost (24). In these cells, Aurora B kinase inhibition induced rapid cell death due to a dependence on an alternate checkpoint function. It would be interesting to explore whether Aurora B kinase inhibition induces rapid DLBCL cell death through noncanonical signaling dependencies linked to RB function or other mechanisms.

DLBCL can present as both a solid tumor mass and disease disseminated in the peripheral blood and other associated tissues. It is therefore critical to target cells in both environments. AZD2811 nanoparticle was efficacious in both the subcutaneous xenograft model OCI-LY19, as well as in the disseminated model U2932. In both models, efficacy was maintained with repeated administration of AZD2811 nanoparticle; however, rapid regrowth was observed at time points that would be consistent with loss of target cover. This suggests that, at least as monotherapy, continuous dosing is required to maximize the therapeutic benefit in these aggressive tumor models. Therefore, establishing how flexible the dose and schedule can be is important, especially if combination therapy is to be introduced.

To this end, the highly aggressive but sensitive model OCI-LY19 was used to explore efficacy as rapid regrowth would occur once target inhibition was lost. The data suggest that administering a similar AZD2811 nanoparticle dose over time using a range of differentiated schedules results in similar antitumor activity. In this aggressive preclinical model, the nanoparticle could maintain efficacy even when dosed once weekly. This flexibility in

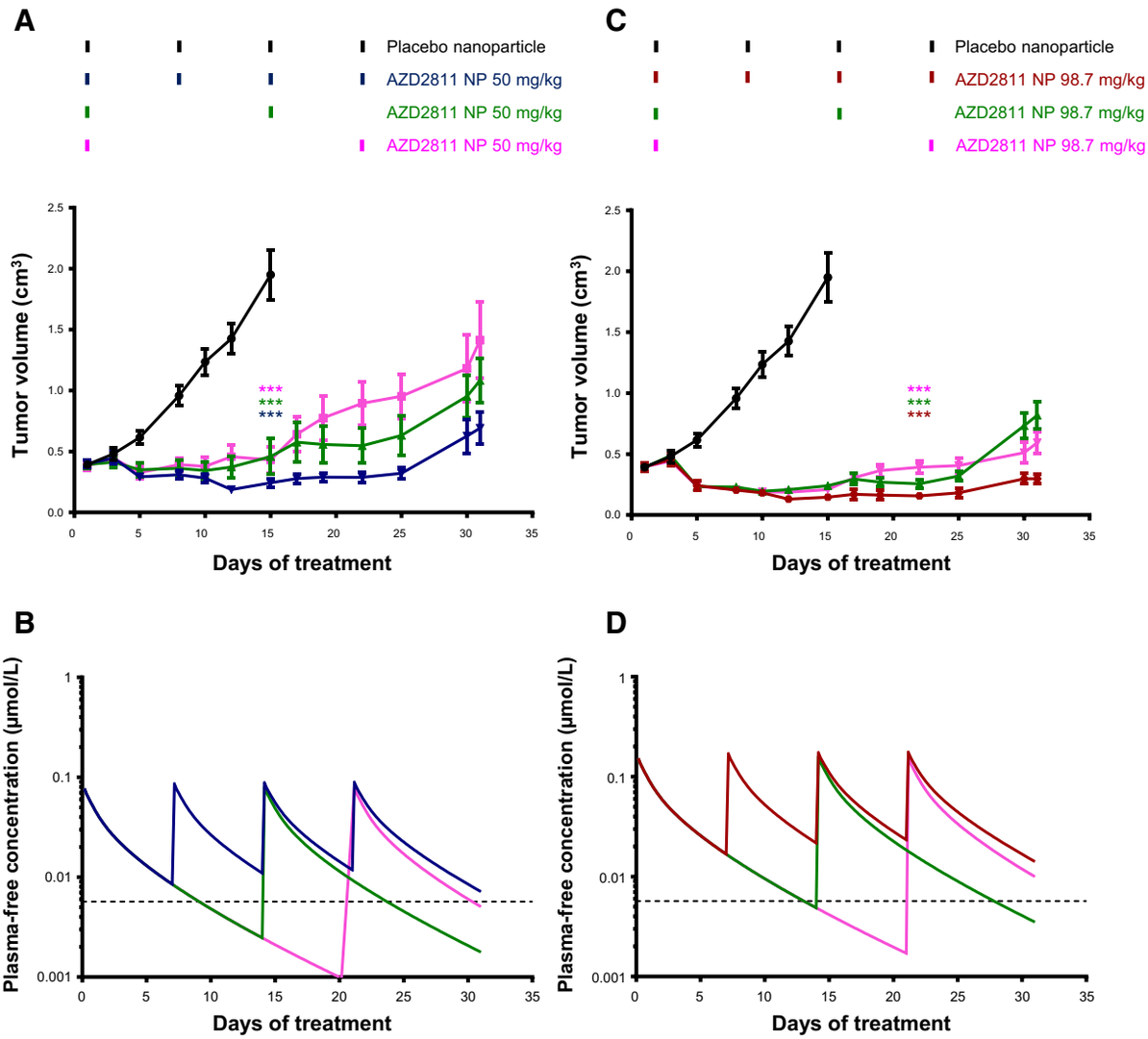

Figure 6.

A reduction of the frequency of dosing of AZD2811 nanoparticle correlates with a reduction of the tumor growth inhibition in the OCI-LY19 DLBCL xenograft model *in vivo*. **A,** Tumor growth inhibition (**A**) and predicted released free concentration profile (**B**) after dosing AZD2811 nanoparticle at 50 mg/kg weekly, or every 2 weeks or every 3 weeks in the subcutaneous OCI-LY19 xenograft model in CB17 SCID mice. **C** and **D,** Tumor growth inhibition (**C**) and predicted released free concentration profile (**D**) after dosing AZD2811 nanoparticle at 98.7 mg/kg weekly, or every 2 weeks or every 3 weeks in the subcutaneous OCI-LY19 xenograft model in CB17 SCID mice. Data are represented as mean ± SEM ($n = 12$ for placebo nanoparticle and $n = 7$ or 8 for AZD2811 nanoparticle-treated groups). Statistical significance was evaluated using a one-tailed *t*-test (***, $P > 0.001$).

application of the nanoparticle builds confidence that different dose schedules could also be effective in the clinical setting (because the release rate of AZD2811 from the nanoparticle controls the duration of Aurora B kinase inhibition and is likely to be equivalent in humans and mice). This would allow administration of the drug to be scheduled according to the patient's health status without compromising the therapeutic response. Using the OCI-LY19, we also demonstrated that increasing the dose delivered led to an increase of the durability of response. Although the *in vivo* studies presented were not designed to look at overall survival, the results suggest that both continuous dosing and dose of nanoparticle drive longer duration of benefit, which would be expected to translate to greater overall survival.

AZD2811 nanoparticle dosed at 25 and 98.7 mg/kg induced rapid apoptosis in the OCI-LY19 model, with 98.7 mg/kg being more effective than 25 mg/kg. However, when AZD2811 nanoparticle is administered using doses and schedules that maintain a similar amount of drug in a dosing cycle then equivalent efficacy was observed. This is consistent with AZD2811 released from the nanoparticle formulation maintaining sufficient target cover to sustain effective inhibition of Aurora B kinase function. This suggests that duration of Aurora B kinase inhibition is the important driver of antitumor efficacy.

A number of studies have also shown that Aurora A kinase inhibitors can be used to target DLBCL (25). In particular, the mixed Aurora A/B kinase inhibitor alisertib has demonstrated

clinical activity in combination with R-CHOP (26). Many of the Aurora A kinase inhibitors have reduced but relevant potency against Aurora B kinase (27). When administered at higher doses, the compound will achieve exposures (clinically or preclinically) sufficient to target both Aurora A and B kinase. Detailed comparative mechanistic studies are required to delineate the specific role for Aurora A and B kinases in more detail. Moreover, careful consideration of the drivers of response through targeting Aurora A or B kinase alone or by inhibition of both is important. It cannot be excluded that in some cell lines, Aurora A kinase function could provide a resistance mechanism following inhibition of Aurora B kinase; however, no studies have addressed this.

Previously, it has been shown that Aurora B kinase is overexpressed in c-Myc–driven B-cell lymphomas that are resistant to standard R-CHOP chemotherapy (19, 28). An *in vitro* study has suggested that vincristine, one of the four standard chemotherapy agents used in R-CHOP, stimulated the phosphorylation of Aurora B kinases (29). In addition, some *in vitro* and *in vivo* data showed that AZD1152 enhanced the ability of vincristine to inhibit proliferation of leukemic cells (29, 30). Unfortunately, it is difficult to model the combination of AZD2811 nanoparticle with R-CHOP in preclinical studies as it requires treating a single animal with 6 different agents. However, we believe that the combination of R-CHOP and AZD2811 nanoparticle could benefit patients and merits clinical investigation.

Thus far, emerging clinical data have not successfully identified patient populations most likely to respond to barasertib. Further work is necessary to identify predictive markers enabling selection of patient subgroups most likely to benefit from AZD2811 nanoparticle treatment and helping to improve the efficiency of future clinical trials.

In summary, these data suggest that the inhibition of Aurora B kinase may represent a new therapeutic strategy in the treatment of DLBCL patients. The AZD2811 nanoparticle formulation has the potential to increase efficacy at tolerable doses while providing greater flexibility in treatment delivery.

Disclosure of Potential Conflicts of Interest

All authors are current or former AstraZeneca employees and shareholders.

Authors' Contributions

Conception and design: N. Floc'h, D. Ferguson, E.J. Pease, S.T. Barry
Development of methodology: N. Floc'h, D. Ferguson, N.J. Curtis
Acquisition of data (provided animals, acquired and managed patients, provided facilities, etc.): N. Floc'h, S. Ashton, P. Taylor, A.M. Hughes, E. Harris, M. Hattersley, S. Wen, J.E. Pilling, L.A. Young
Analysis and interpretation of data (e.g., statistical analysis, biostatistics, computational analysis): N. Floc'h, D. Ferguson, L.S. Carnevalli, M. Hattersley, N.J. Curtis, J.E. Pilling, L.A. Young, K. Maratea, E.J. Pease, S.T. Barry
Writing, review, and/or revision of the manuscript: N. Floc'h, D. Ferguson, L.S. Carnevalli, M. Hattersley, J.E. Pilling, L.A. Young, S.T. Barry
Administrative, technical, or material support (i.e., reporting or organizing data, constructing databases): N. Floc'h, P. Taylor, E. Harris, N.J. Curtis
Study supervision: N. Floc'h, S. Ashton, P. Taylor

Acknowledgments

We thank staff in Laboratory Animal Sciences in Alderley Park and Gatehouse Park for technical support, Aaron Smith and Joanne Wilson for their work supporting the build of the PK model, and BIND Therapeutics Inc. for providing the nanoparticle formulations.

The costs of publication of this article were defrayed in part by the payment of page charges. This article must therefore be hereby marked *advertisement* in accordance with 18 U.S.C. Section 1734 solely to indicate this fact.

Received June 28, 2018; revised December 3, 2018; accepted March 7, 2019; published first March 14, 2019.

References

1. Swerdlow SH, Campo E, Harris NL, Jaffe ES, Pileri SA, Stein H, et al. WHO Classification of Tumours of Haematopoietic and Lymphoid Tissues. Lyon, France: IARC Press; 2008.
2. Alizadeh AA, Eisen MB, Davis RE, Ma C, Lossos IS, Rosenwald A, et al. Distinct types of diffuse large B-cell lymphoma identified by gene expression profiling. Nature 2000;403:503–11.
3. Rosenwald A, Wright G, Chan WC, Connors JM, Campo E, Fisher RI, et al. The use of molecular profiling to predict survival after chemotherapy for diffuse large-B-cell lymphoma. N Engl J Med 2002;346:1937–47.
4. Sehn LH, Donaldson J, Chhanabhai M, Fitzgerald C, Gill K, Klasa R, et al. Introduction of combined CHOP plus rituximab therapy dramatically improved outcome of diffuse large B-cell lymphoma in British Columbia. J Clin Oncol 2005;23:5027–33.
5. Vose JM, Link BK, Grossbard ML, Czuczman M, Grillo-Lopez A, Gilman P, et al. Phase II study of rituximab in combination with chop chemotherapy in patients with previously untreated, aggressive non-Hodgkin's lymphoma. J Clin Oncol 2001;19:389–97.
6. Sarkozy C, Coiffier B. Diffuse large B-cell lymphoma in the elderly: a review of potential difficulties. Clin Cancer Res 2013;19:1660–9.
7. Pasqualucci L, Dalla-Favera R.The genetic landscape of diffuse large B-cell lymphoma. Semin Hematol 2015;52:67–76.
8. Dunleavy K, Pittaluga S, Czuczman MS, Dave SS, Wright G, Grant N, et al. Differential efficacy of bortezomib plus chemotherapy within molecular subtypes of diffuse large B-cell lymphoma. Blood 2009;113:6069–76.
9. Liu D, Mamorska-Dyga A. Syk inhibitors in clinical development for hematological malignancies. J Hematol Oncol 2017;10:145.
10. Wilson WH, Young RM, Schmitz R, Yang Y, Pittaluga S, Wright G, et al. Targeting B cell receptor signaling with ibrutinib in diffuse large B cell lymphoma. Nat Med 2015;21:922–6.
11. Paul J, Soujon M, Wengner AM, Zitzmann-Kolbe S, Sturz A, Haike K, et al. Simultaneous inhibition of PI3Kδ and PI3Kα induces ABC-DLBCL regression by blocking BCR-dependent and -independent activation of NF-κB and AKT. Cancer Cell 2017;31:64–78.
12. Mounier N, Briere J, Gisselbrecht C, Emile JF, Lederlin P, Sebban C, et al. Rituximab plus CHOP (R-CHOP) overcomes bcl-2–associated resistance to chemotherapy in elderly patients with diffuse large B-cell lymphoma (DLBCL). Blood 2003;101:4279–84.
13. Knutson SK, Warholic NM, Johnston LD, Klaus CR, Wigle TJ, Iwanowicz D, et al. Synergistic anti-tumor activity of EZH2 inhibitors and glucocorticoid receptor agonists in models of germinal center non-Hodgkin lymphomas. PLoS One 2014;9:e111840.
14. Morin RD, Johnson NA, Severson TM, Mungall AJ, An J, Goya R, et al. Somatic mutations altering EZH2 (Tyr641) in follicular and diffuse large B-cell lymphomas of germinal-center origin. Nat Genet 2010;42:181–5.
15. Ashton S, Song YH, Nolan J, Cadogan E, Murray J, Odedra R, et al. Aurora kinase inhibitor nanoparticles target tumors with favorable therapeutic index *in vivo*. Sci Transl Med 2016;8:325ra17.
16. Boss DS, Witteveen PO, van der Sar J, Lolkema MP, Voest EE, Stockman PK, et al. Clinical evaluation of AZD1152, an i.v. inhibitor of Aurora B kinase, in patients with solid malignant tumors. Ann Oncol 2011;22:431–7.
17. Mortlock AA, Foote KM, Heron NM, Jung FH, Pasquet G, Lohmann JJ, et al. Discovery, synthesis, and *in vivo* activity of a new class of pyrazoloquinazolines as selective inhibitors of aurora B kinase. J Med Chem 2007;50:2213–24.
18. Wilkinson RW, Odedra R, Heaton SP, Wedge SR, Keen NJ, Crafter C, et al. AZD1152, a selective inhibitor of Aurora B kinase, inhibits human

tumor xenograft growth by inducing apoptosis. Clin Cancer Res 2007; 13:3682–8.
19. Yang D, Liu H, Goga A, Kim S, Yuneva M, Bishop JM. Therapeutic potential of a synthetic lethal interaction between the MYC proto-oncogene and inhibition of aurora-B kinase. Proc Natl Acad Sci U S A 2010;107: 13836–41.
20. Ditchfield C, Johnson VL, Tighe A, Ellston R, Haworth C, Johnson T, et al. Aurora B couples chromosome alignment with anaphase by targeting BubR1, Mad2, and Cenp-E to kinetochores. J Cell Biol 2003;161:267–80.
21. Collins GP, Eyre TA, Linton KM, Radford J, Vallance GD, Soilleux E, et al. A phase II trial of AZD1152 in relapsed/refractory diffuse large B-cell lymphoma. Br J Haematol 2015;170:886–90.
22. Kilkenny C, Browne WJ, Cuthill IC, Emerson M, Altman DG. Improving bioscience research reporting: the ARRIVE guidelines for reporting animal research. PLoS Biol 2010;8:e1000412.
23. Shalgunov V, Zaytseva-Zotova D, Zintchenko A, Levada T, Shilov Y, Andreyev D, et al. Comprehensive study of the drug delivery properties of poly(l-lactide)-poly(ethylene glycol) nanoparticles in rats and tumor-bearing mice. J Control Release 2017;261:31–42.
24. Gong X, Du J, Parsons SH, Merzoug FF, Webster Y, Iversen PW, et al. Aurora-A kinase inhibition is synthetic lethal with loss of the *RB1* tumor suppressor gene. Cancer Discov 2019;9:248–63.
25. Friedberg JW, Mahadevan D, Cebula E, Persky D, Lossos I, Agarwal AB, et al. Phase II study of alisertib, a selective Aurora A kinase inhibitor, in relapsed and refractory aggressive B- and T-cell non-Hodgkin lymphomas. J Clin Oncol 2014;32:44–50.
26. Kelly KR, Friedberg JW, Park SI, McDonagh K, Hayslip J, Persky D, et al. Phase I study of the investigational Aurora A kinase inhibitor alisertib plus rituximab or rituximab/vincristine in relapsed/refractory aggressive B-cell lymphoma. Clin Cancer Res 2018;24:6150–9.
27. Gavriilidis P, Giakoustidis A, Giakoustidis D. Aurora kinases and potential medical applications of Aurora kinase inhibitors: a review. J Clin Med Res 2015;7:742–51.
28. den Hollander J, Rimpi S, Doherty JR, Rudelius M, Buck A, Hoellein A, et al. Aurora kinases A and B are up-regulated by Myc and are essential for maintenance of the malignant state. Blood 2010;116:1498–505.
29. Ikezoe T, Takeuchi T, Yang J, Adachi Y, Nishioka C, Furihata M, et al. Analysis of Aurora B kinase in non-Hodgkin lymphoma. Lab Invest 2009; 89:1364–73.
30. Yang J, Ikezoe T, Nishioka C, Tasaka T, Taniguchi A, Kuwayama Y, et al. AZD1152, a novel and selective aurora B kinase inhibitor, induces growth arrest, apoptosis, and sensitization for tubulin depolymerizing agent or topoisomerase II inhibitor in human acute leukemia cells *in vitro* and *in vivo*. Blood 2007;110:2034–40.